Environmental Science & Technology

pubs.acs.org/est

Article

Enhanced Rates of Transition-Metal-Ion-Catalyzed Oxidation of S(IV) in Aqueous Aerosols: Insights into Sulfate Aerosol Formation in the Atmosphere

Kyle J. Angle, Erin E. Neal, and Vicki H. Grassian*

Cite This: https://doi.org/10.1021/acs.est.1c01932

Read Online

ACCESS | Metrics & More | Article Recommendations | Supporting Information

ABSTRACT: The oxidation of S(IV) is a critical step in the fate of sulfur dioxide emissions that determines the amount of sulfate aerosol in the atmosphere. Herein, we measured accelerated S(IV) oxidation rates in micron-sized aqueous aerosols compared to bulk solutions. We have investigated both buffered and unbuffered systems across a range of pH values in the presence of atmospherically relevant transition-metal ions and salts and consistently found the oxidation rate to be accelerated by ca. 1−2 orders of magnitude in the aerosol. This enhancement is greater than can be explained by the enrichment of species in the aerosol compared to the bulk and indicates that surface effects and potentially aerosol pH gradients play important roles in the S(IV) oxidation process in the aqueous aerosol. In addition, our experiments were performed with dissolved S(IV) ions (SO_3^{2-}/HSO_3^-), allowing us to demonstrate that acceleration occurs in the condensed phase showing that enhanced sulfate formation is not exclusively due to gas-aerosol partitioning or interfacial SO_2 oxidation. Our findings are an important step forward in understanding larger than expected sulfate concentrations observed in the atmosphere and show that inorganic oxidation processes can be accelerated in micron-sized aqueous droplets compared to the bulk solution.

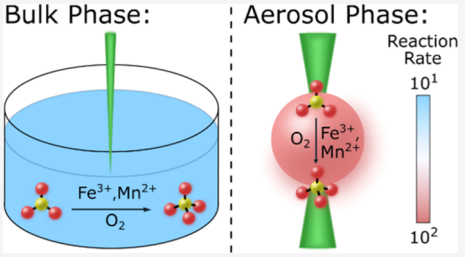

KEYWORDS: *reaction acceleration, sulfur chemistry, aerosol pH, surface access, kinetics, optical tweezers, ionic strength, sulfite*

1. INTRODUCTION

The oxidation of S(IV) is a key reaction in atmospheric chemistry. Sulfur dioxide (SO_2) is emitted from individual sources at rates as large as 4000 kilotons per year.[1] The continental background concentration of SO_2 is up to 1 part per billion (ppb) and polluted regions can have levels of several hundred ppb.[2] In the atmosphere, SO_2 dissolves into aqueous systems including aerosols and cloud droplets to form one of several aqueous S(IV) species, including bisulfite (HSO_3^-), sulfite (SO_3^{2-}), and metabisulfite ($S_2O_5^{2-}$), which hereafter will be collectively termed $S(IV)_{aq}$. These species are oxidized by a variety of pathways into sulfate (SO_4^{2-}). For example, for bisulfite, the oxidation reaction with oxygen can be written as

$$HSO_3^- + \frac{1}{2}O_2 \rightarrow SO_4^{2-} + H^+ \quad (1)$$

This reaction can impact the composition and acidity of atmospheric aerosols. Although the oxidation of S(IV) is relatively slow, this is critically important to environmental chemistry, as the pH of aerosols and cloud droplets influences the rate of acid-catalyzed chemical transformations, the impact of aerosols on human health, and even the ability of aerosols to act as cloud condensation nuclei.[3−5]

The oxidation of $S(IV)_{aq}$ is overall quite complex and notoriously sensitive to reaction conditions. In addition, recent measurements have shown more formation of sulfate during severe pollution events than can be accounted for by current models.[6,7] The process is highly pH-dependent, with different rate laws and mechanisms operative for different pH regimes (acidic, neutral, and basic).[8] The reaction is also inhibited by many different chemical species, including organic compounds, ammonia, and even S(IV) itself.[9,10] These all vary with ionic strength, μ, and depending on the exact conditions, higher μ can either accelerate or inhibit the reaction kinetics.[10−12] Furthermore, the reaction can be catalyzed by transition-metal ions (TMIs).[10,13] TMI-catalyzed oxidation can, under some circumstances, be the dominant pathway of sulfate formation in the atmosphere.[14] Indeed, one study found that the reaction is seven times faster in distilled water versus Milli-Q water due to the presence of TMIs in distilled water, despite the fact that these are present in sub-micromolar concentrations.[15]

Since the reaction rate depends on the exact nature of the solution matrix, and more sulfate is being observed in haze

Received: March 26, 2021
Revised: July 4, 2021
Accepted: July 6, 2021

events than can be explained by current kinetics data, the current study focuses on high ionic strengths (μ > 2 M) found in aerosols to help fulfil the need for solute-strength-dependent kinetics in this regime.[12,16,17] We also worked in the 0.1−1.5 m $S(IV)_{aq}$ range since the majority of studies on S(IV) oxidation have utilized concentrations on the order of 0.01 m or less (note: "m" refers to molality throughout this report).[10,18,19] Even higher concentrations are not practical since the saturation concentration of Na_2SO_3 is 2.1 M.[20] We employed Aerosol Optical Tweezers (AOT) to suspend individual droplets in surface-free environments and to continuously monitor their composition, size, and refractive index via Raman spectroscopy and Whispering Gallery Modes (WGMs).[21] We used confocal Raman spectroscopy to monitor the same systems in the bulk phase. This allowed us to use our single-aerosol measurements to determine the extent to which oxidation of $S(IV)_{aq}$ catalyzed by TMIs and common salts is accelerated in aerosols as well as the pH dependence of this process.

2. MATERIALS AND METHODS

2.1. Materials. All solutions were prepared using milliQ water with a resistivity >18.1 MΩ. Sodium chloride (Fisher Lot 188772 and 186819) and sodium sulfate (Fisher Lot 161950) were baked at 200 °C for at least 48 h to remove organic impurities. Buffers were prepared from sodium acetate (Macron Batch 0000227236), imidazole (Sigma-Aldrich Lot WXBC9930V), glacial acetic acid (Fisher Lot 200447), and 1 and 6 N HCl (Fisher Lot 195295 and 183144). The pH of solutions was measured with a pH meter (OAKTON Instruments) and ranged from pH 5.4 to 9.4 ± 0.3 for unbuffered experiments and was either 7.0 or 3.8 ± 0.1 for buffered experiments. For experiments with added Fe and Mn, $FeCl_3{\cdot}6H_2O$ (Aldrich Lot MKBC9551V) and $MnCl_2{\cdot}4H_2O$ (Fisher Lot 162637) were used, respectively. Various sources of S(IV), including $NaHSO_3^-$ (bisulfite), $Na_2S_2O_5$ (meta-bisulfite), and Na_2SO_3 (sulfite) were used to verify that aerosol-phase acceleration was not unique to one lot number, and these sources are listed in Table S1 in the Supporting Information. Additional reagents included sodium nitrate (Sigma-Aldrich Lot MKBW8240V) and sodium perchlorate (Sigma-Aldrich 0401080). Except where otherwise noted, salts were used to adjust the ionic strength to 2.45 m.

2.2. Methods. For bulk experiments, a confocal Raman spectrometer (HORIBA) was used with the LabSpec 8 software suite. Solutions were prepared by first weighing the S(IV) source and any salts such as NaCl into a scintillation vial and then adding Milli-Q water and acid or buffer as needed to obtain the appropriate pH. Solutions were agitated vigorously to quickly dissolve the solids, and this likely resulted in solutions with dissolved O_2 at saturation for the given temperature (23.5 ± 0.5 °C) and ionic strength. 5 mL of the solution was pipetted into a glass Petri dish, and Kimwipe (Kimberly-Clark) fibers were gently dusted onto the surface of the solution to aid in laser focusing. Spectra were obtained with 10 s acquisition times and five accumulations, typically every 3 min for an average of 67 min total, using 1800 grooves/millimeter for optimal resolution. For reaction times greater than an hour, the laser occasionally was refocused on the solution surface due to water evaporation. For experiments with sodium nitrate, the nitrate peak was used as an internal standard to track the relative intensity of the spectra over time. By focusing the laser slightly past the surface, the intensity of the signal remains relatively constant for over an hour as the evaporation causes the laser focus to pass through the optimal position, and then the signal begins to decrease with further evaporation (see Figure S1 in the Supporting Information).

For experiments in the aerosol phase, a pair of commercial Aerosol Optical Tweezers 100 (Biral Inc.) was used. Solutions were prepared the same as for the bulk and then aerosolized by an ultrasonic nebulizer (MicroAIR U22, OMRON), resulting in aerosols 3 ± 1 μm in radius. The aerosols were trapped by a laser (532 nm, 50 mW power). Except where stated otherwise, the relative humidity (RH) was maintained at 90 ± 8% by a controlled flow of wet and dry nitrogen gas (total flow 30 sccm). The amount of O_2 present in the chamber was less than ambient conditions due to the N_2 flow, and data used to estimate the O_2 concentration are given in Figure S11. Raman spectra were acquired every second at 1200 g/millimeter and averaged in sets of 11 for analysis. Temperature probe readings were 24.6 ± 0.1 °C, and additional heating of the aerosol by the laser is expected to be on the order of 100 mK.[22] The Raman spectrometer wavenumbers were calibrated using standard emission lines from a Hg and Ne/Ar USB light source (Princeton Instruments). Average experiments included 12 min of S(IV)-containing aerosol data, followed by external standard(s). Calibration of intensity was performed by trapping a ca. 1 m sodium sulfate and/or nitrate aerosol for the acquisition of at least 100 spectra at the end of every experiment and quantifying the aerosol-phase concentration by obtaining refractive index. This allowed the determination of the concentration of sulfate in other samples from that experiment via comparison of the integrated area of the sulfate peak (982 cm^{-1}) or nitrate peak (1049 cm^{-1}).

Details of other measurements are given in the Supporting Information. Briefly, TMI concentrations were quantified using a Thermo Fisher iCAP RQ ICP−MS analyzer. Bulk-phase refractive index measurements were performed using an ABBE-3L refractometer (Bausch & Lomb). Finally, enrichment factors (EFs) were measured by AOT, conductivity probe, and inductively coupled plasma mass spectrometry (ICP−MS) methods.

3. RESULTS

3.1. Spectral Evidence of Acceleration. Representative Raman spectra of the oxidation reaction at acidic pH are given in Figure 1. The sulfate band is located at 982 cm^{-1} and has the same location within spectral resolution for both phases. In addition, HSO_3^- and $S_2O_5^{2-}$ peaks are present at higher

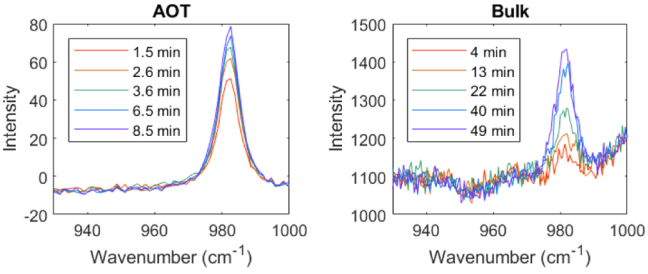

Figure 1. Representative sulfate ion spectra as a function of time. Each trace shows Raman spectra following the formation of sulfate in aerosol and bulk phases at pH 5.6. The solutions contained 1.0 m S(IV) and 0.2 m $NaNO_3$. The aerosol was 4.0 μm in radius, and the bulk solution was 5 mL in a glass Petri dish (d = 55 mm) exposed to ambient O_2.

https://doi.org/10.1021/acs.est.1c01932
Environ. Sci. Technol. XXXX, XXX, XXX−XXX

wavenumbers, 1025 and 1052 cm^{-1} (see Figure S2 in the Supporting Information). At high pH (≥7), for bulk spectra, there are broad, overlapping SO_3^{2-} bands at 953 and 967 cm^{-1} (see Figure S2). By contrast, for aerosol-phase spectra at all pH values, the S(IV) bands have low intensity. This is consistent with our previous work with the SO_4^{2-}/HSO_4^- system, where the latter had substantially lower intensity relative to sulfate in the aerosol compared to the bulk.[23] The S(IV) bands do appear when sufficient S(IV) is dissolved in the bulk solution and aerosols with high S(IV) concentrations generated from these solutions are trapped (as shown in Figure S2).

Figure 1 also shows that sulfate peaks are present in the AOT spectra as soon as the micron-sized aerosol is trapped in the optical tweezers and grow in intensity faster than that seen in the bulk-phase spectra. The aerosol is prepared by nebulization of a bulk solution and is trapped within 5 min of beginning the experiment. Fewer than 30 s pass between aerosol trapping and spectral acquisition. It is clear that some of this sulfate formation is occurring during the trapping process. The rate of sulfate formation is then determined using only the data after the aerosol is stabilized in the AOT. For example, for the AOT data shown in Figure 1, the first data point used in computing rate is obtained from the first spectrum, not from [sulfate] = 0. Likewise, for calculating bulk-phase rates, the first data point used is obtained from the first spectrum where sulfate peak area can be calculated by Gaussian curve fitting. The advantage of this method is that it makes the results less sensitive to any sulfate already present in the S(IV) source and it excludes interference from an induction period.[10,24,25]

3.2. Quantifying Apparent Acceleration Factors for Various Conditions. For both bulk and aerosol spectra, sulfate concentrations were calculated using calibration curves (see Figures S3 and S4 in the Supporting Information). We found that sulfate formation is significantly faster in the aerosol phase than in the bulk. To quantify this acceleration, we defined an apparent acceleration factor (AAF) as given in eq 2

$$\mathrm{AAF} = \frac{r_a}{r_b} \tag{2}$$

Here, r_a and r_b are the rates (in m/min) observed in the aerosol and bulk phases, respectively, where sulfate formation was linear with time. The data included in our rates began with the first spectrum containing a stable, quantifiable sulfate peak and ended after sufficient data were obtained (see Supporting Information, Discussion on rate computation for details). Representative linear fits are given in Figure 2.

A summary of AAFs for different experimental conditions is given in Table 1, with full details in Table S1. Here, a "data set" is the result from one bulk-phase experiment compared to the average of multiple aerosol-phase experiments with all parameters held constant. We tested a wide variety of pH conditions to determine the impact of this parameter on the AAF, with particular emphasis on acidic conditions since the majority of atmospheric aerosols are acidic.[3,26] Even for unbuffered experiments, changes in pH during the reaction are expected to be small (<0.1 pH unit) since the large concentrations of SO_3^{2-} would absorb the majority of protons produced from the oxidation.[27] Ionic strength was controlled using either NaCl or $NaNO_3$, two relevant salts for atmospheric aerosols.[3,12,16] AAFs show that the reaction is at least an order of magnitude faster in the aerosol phase. Additionally, we computed an apparent acceleration factor corrected for enrichment (AAFE) to account for the increased ionic strength and reagent concentrations in the aerosol (see Supporting Information). In all cases, AAFEs are larger than AAFs by 19−477 percent.

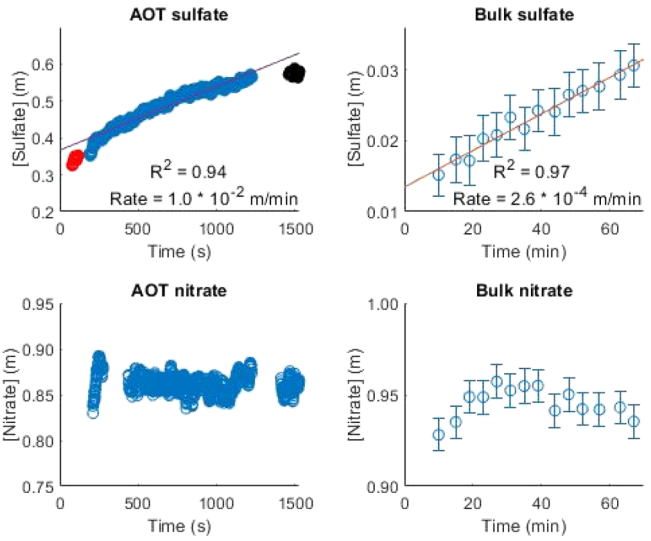

Figure 2. Sample sulfate formation data for the aerosol and bulk phases. The data are from pH 9.4 samples with 1 m Na_2SO_3 and 0.95 m $NaNO_3$ as the internal standard. AOT data show consecutive averages of 11 spectra (e.g., circles show spectra 1−11, 2−12, 3−13, etc.). Gaps in AOT data correspond to interference from WGMs; internal standard data with WGMs is given in Figure S1. The aerosol data was collected for longer than a typical experiment to demonstrate the extent of linearity of sulfate formation, and initial data corresponding to aerosol stabilization (red circles) as well as data departing from linearity (black circles) are not included in rate computation. AOT data error bars are not shown for clarity and are ca. ± 0.02 m. Bulk error bars show the error in the sulfate band area from peak fitting.

Table 1. Summary of AAFs for S(IV) Oxidation in the Aerosol vs Bulk Phase under Different pH Conditions[a]

pH conditions	number of data sets	[S(IV)] (m)	Avg AAF	AAF range	AAFE range
acidic unbuffered	18	1.0	19	4−45	7−57
neutral unbuffered	5	1.0	33	10−55	12−96
basic unbuffered	10	1.0	41	15−92	21−153
pH 3.8 acetate buffer	4	0.5−1.4	55	41−78	48−89
pH 7.0 imidazole buffer	10	0.2−0.4	33	14−76	16−163

[a]See Table S1 in the Supporting Information for more detailed conditions used.

For our systems, since we worked at high concentrations of S(IV) and salts, there was sufficient TMI present to catalyze the oxidation as the salt samples contained non-negligible concentrations of TMI. In order to quantify TMI concentrations, ICP−MS was employed to measure iron, manganese, copper, and cobalt amounts in our samples (Table S1). To further probe the nature of TMI catalysis, we performed experiments with explicitly added Fe^{3+} or Mn^{2+}. In both cases, S(IV) oxidation remained faster in the aerosol phase than the bulk across the pH range we studied (5.4−9.3). It is noteworthy that iron speciation changes considerably over this range, and therefore, our results show that S(IV) oxidation

https://doi.org/10.1021/acs.est.1c01932
Environ. Sci. Technol. XXXX, XXX, XXX−XXX

acceleration occurs with different TMI species present.[28,29] Table 1 also shows that AAFs generally increase with pH for unbuffered systems.

For buffered experiments, the pH was maintained at either 3.8 or 7.0 with an acetate or imidazole buffer, respectively, and $[S(IV)]_{aq}$ was varied. For the imidazole systems, AAFs went through a maximum at ca. 0.3 m S(IV). At relatively high S(IV) concentrations (0.4 m), additional S(IV) increases the rate to a lesser extent due to self-inhibition (Figure S5d). For the acetate systems, it was necessary to work at higher concentrations so the sulfate Raman band could be used to obtain multiple data points before acetic acid evaporation from the aerosol compromised the buffer pH. At these concentrations, any trend between AAF and [S(IV)] is less obvious. This may also be due to the complexity of the factors involved, namely, acid catalysis and inhibition by acetate.[9,30] Even so, consistent acceleration in the aerosol versus the bulk is observed over a wide range of conditions.

3.3. Measurement of Aerosol-Phase Concentrations.

Aerosol concentrations were measured by using the refractive index (n) of optically trapped aerosols to calculate their total solute content as has been previously demonstrated.[31] From the position and spacing of WGMs (Figure 3), n can be precisely obtained.[21] This enables the calculation of molal refractivity (R) and hence mole fraction of solute x as shown in eqs 3−5

$$R = R_w + x(R_s - R_w) \quad (3)$$

$$R = \frac{n^2 - 1}{n^2 + 2} * x(M_w + (M_s - M_w)) * \frac{1}{d} \quad (4)$$

$$d = d_0 + \sum_i A_i * x^i \quad (5)$$

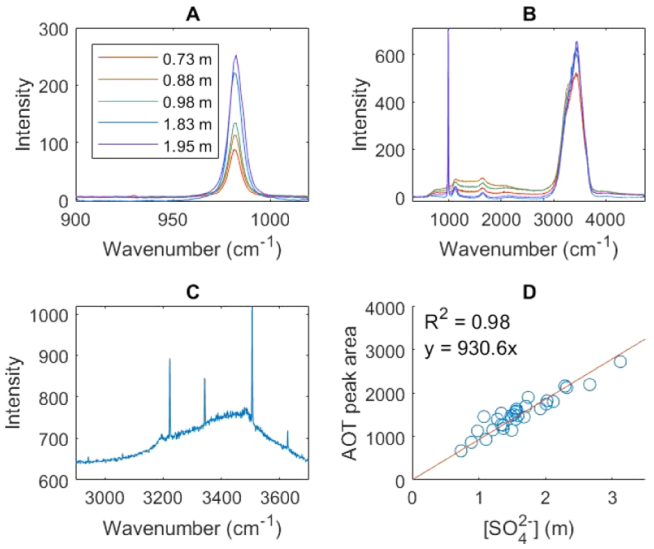

Figure 3. (A) sample Na_2SO_4 AOT spectra taken at 1200 grooves/mm in the sulfate region showing the concentration-dependence of the prominent sulfate peak at 982 cm^{-1}; (B) same aerosols as "A" taken at 300 grooves/mm to show the entire spectral range (A,B both show averages of 11 spectra, so WGMs are not visible); (C) single spectrum taken at 1200 grooves/millimeter in the water O−H stretching region showing the WGMs, used to calculate aerosol size and refractive index, that appear on the broader water peak; and (D) calibration curve relating Raman peak area to sulfate ion concentration calculated by refractive index. The fit line has a set intercept of (0, 0).

Here, R_w, R_s and M_w, and M_s are the refractivities and molar masses of water and the average solute, respectively, d is the density of the solution, d_0 is the density of pure water, and A_i are density polynomial coefficients. Refractivities were determined using a refractometer, and A_i values were taken from the literature.[32,33] When the solute is a salt, the M_s is the weighted average molar mass of its ions. When eqs 3 and 4 are set equal to solve for x, an algebraic solution does not exist. Thus, calculations were performed by checking every possible x in small increments across a physically realistic range and keeping the solution with the least difference between eqs 3 and 4.

For a given n, there is one possible x, allowing calculation of aerosol-phase concentration for systems containing one binary salt. When multiple salts are present, however, these equations do not have a single solution since the enrichments of the salts may be different and hence the salts may be present in different ratios in the aerosol than as prepared in the bulk. Therefore, independent measurements of the concentrations of all but one salt are necessary to uniquely determine the concentration of all species in the aerosol phase. For our work, we used NaCl, Na_2SO_4, and $NaNO_3$, the latter two of which have distinct Raman bands, allowing concentration to be determined via calibration curves (Figures S3 and S4). From aerosol concentration, an EF can be calculated, which here we simply define as the aerosol-phase concentration of a species divided by the concentration in the bulk from which the aerosol was generated. EFs were also calculated by ICP−MS and conductivity experiments as outlined in the Supporting Information.

3.4. Impact of Ionic Strength.

Both NaCl and $NaNO_3$ were found to be enriched in the aerosol phase, so it is important to account for the impact this has on the oxidation rate. To this end, we performed several series of bulk-phase experiments where salt concentration could be precisely controlled, and the results are given in Figure 4. It is clear that increasing [NaCl] or $[NaNO_3]$ would not increase the oxidation rate, and in fact, their enrichment actually slows the oxidation down. The difference in intercepts for the linear fits is not a concern since the NaCl experiments used 0.2 m $NaNO_3$ as an internal standard, while the $NaNO_3$ experiments used no NaCl. The experiments with NaCl and $NaNO_3$ were also performed in the aerosol phase (Figure S6 in the Supporting Information) and indicate the same trend. To determine if this effect was simply due to increased ionic strength, we also tested the impact of sodium perchlorate ($NaClO_4$) on the rate, as this ion is generally considered inert toward these types of reactions.[34] Figure 4C shows that $NaClO_4$ has the most negative impact on the rate out of the three salts, with a less linear relationship. Taking the same data and plotting the log of the rate versus an ionic strength parameter defined as $\mu^{1/2}/(1+\mu^{1/2})$, a more linear result is obtained in Figure 4D; this is consistent with previous work on the impact of ionic strength on aqueous TMI-catalyzed S(IV) oxidation.[30]

4. DISCUSSION

Recent studies have shown the acceleration of reactions in aerosols. This has been the subject of a great deal of interest.[35,36] For reasons that remain not fully understood,

https://doi.org/10.1021/acs.est.1c01932
Environ. Sci. Technol. XXXX, XXX, XXX−XXX

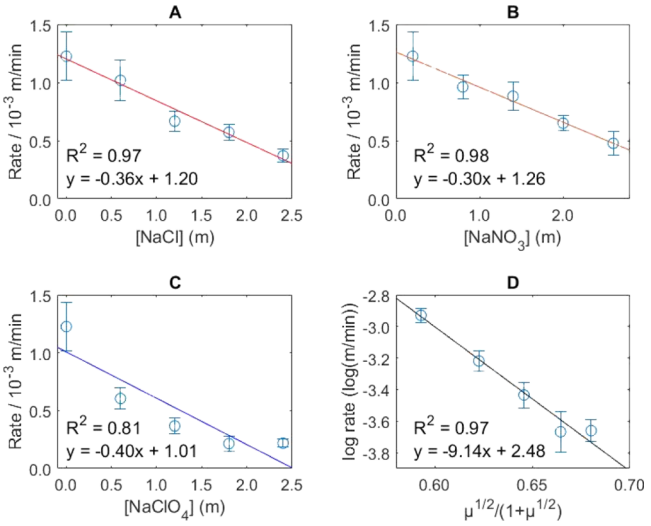

Figure 4. Impact of various anions on sulfur oxidation rates in bulk aqueous solutions of (A) [NaCl]; (B) [$NaNO_3$]; and (C,D) [$NaClO_4$]. All solutions were prepared at pH 5.6. Solutions were composed of 1 m S(IV), the salt indicated by the x-axis, and for all data except (B), 0.2 m $NaNO_3$ was used as an internal standard. (C,D) reflect the same data plotted differently. Error bars show 95% confidence intervals from linear regression of [SO_4^{2-}] vs time.

the environment of picoliter droplets greatly enhances the kinetics of many chemical transformations.[37] Clarke and Radojevic showed that S(IV) oxidation could be substantially faster in sea spray aerosols than in seawater due to catalysis by ions such as Cl^-, although whether this was attributable to the aerosol environment was unclear since the concentrations of Cl^- and H^+ were orders of magnitude larger in their aerosols compared to the bulk.[38] Liu et al. used an aerosol flow tube reactor to find that deliquesced, submicron aerosol droplets enhance the rate of S(IV) oxidation by hydrogen peroxide (and by TMIs at pH 2.8; although this effect is inhibited by increasing ionic strength).[30] Zhang et al. measured SO_2 oxidation by Mn^{2+} and Fe^{3+} using a smog chamber and calculated the reaction to be 2 orders of magnitude faster for oxidation by Mn^{2+}, assuming that the rate law is the same in the bulk and aerosol phases.[11] The studies by both Liu et al. and Zhang et al. were performed under conditions using SO_2 as the S(IV) source, so it is unknown whether the accelerated reaction is $S(IV)_{aq}$ oxidation, interfacial SO_2 (g) oxidation, or both. Indeed, experiments with SO_2 (g) are complicated by the solubility of the gas into aerosols, which depends on pH and μ. Therefore, here we used aqueous S(IV) sources at higher pH levels where the formation of SO_2 does not occur and $S(IV)_{aq}$ oxidation can be isolated. There is also a recent report by Wang et al. demonstrating aerosol-phase acceleration for the Mn-catalyzed pathway via chamber studies up to pH 7.[39] We hope to contribute further to the understanding of S(IV) reaction acceleration by studying the reaction on a single aerosol particle basis.

Although aerosol-phase acceleration is more easily explained for highly charged droplets created from electrospray ionization, acceleration has been shown for uncharged aqueous droplets as well.[36] We note that differences in rates between the bulk phase and the aerosol observed here are not due to diffusion limitations in the bulk, as demonstrated in the Supporting Information, and therefore, other mechanisms are needed to explain accelerated sulfate formation. As discussed in more detail, three relevant factors are considered. The first is the enrichment of species from the bulk to the aerosol phase. This is quantified by EFs (see Results). Second, we will consider the implications of the fact that molecules in the aerosol phase have more access to the surface relative to the bulk phase. Third, we will discuss the impact of pH on the oxidation rate. Finally, we briefly describe how the approach used here for these types of reaction acceleration studies is consistent with some recent recommendations.[40]

4.1. Enrichment. The increase in oxidation rate could theoretically be due to increased concentrations in the aerosol phase. First, we consider this possibility for the NaCl and $NaNO_3$ salts we used. The implication of Figure 4 is that the inhibiting effect of increasing [NaCl] or [$NaNO_3$] is mainly inhibiting due to increasing μ but slightly less inhibiting than a totally inert ion due to the weakly catalyzing nature of NaCl and $NaNO_3$.[40] This can be seen by comparing the slopes of Figure 4a–c. However, the overall effect for both ions is still inhibiting, and therefore, enrichment of these ions into the aerosol phase would not accelerate the reaction. We performed a similar analysis on the enrichment of S(IV) and TMIs and found that, combined, their enrichment would not even double the reaction rate, far below what is found in Table 1 (see Supporting Information, Discussion 2). Therefore, other factors must be the main cause of acceleration.

4.2. Surface Access. In droplets, molecules have greater access to the interface than in bulk solutions. This is quantified by two characteristic lengths. The first is the length of the compartment in which the molecules are confined, L_{com}, and the second is the average distance a molecule travels before reacting, L_{rxn}.[41]

$$L_{rxn} = \sqrt{D^*t} \quad (6)$$

Here, D is the diffusion coefficient and t is the chemical lifetime (the product of the concentration and the inverse of the rate). Using representative values for our system and the diffusion coefficient of sulfite,[42] we found L_{rxn} and L_{com} to be 600 and 8 μm for aerosols and 6200 and 55,000 μm, respectively, for the bulk. This indicates that molecular species present in the aerosols sample the surface several times before reacting, while in the bulk phase, they do not. For this reaction, surface access could accelerate the oxidation process by increasing interaction with ambient O_2 diffusing at the air/water interface. Since the reaction steps proceed at different rates depending on the form of S(IV), surface access could also enhance the process by altering S(IV) speciation.[43] It has been shown that molecules can have distinct surface and bulk pK_a values, so it is reasonable to infer that various S(IV) equilibria can be different at the interface.[27,44] Generally, the more highly charged an ion is, the greater the energy cost to move it to the air–water interface.[45] For our systems, this indicates that $SO_3^{\bullet-}$ is more likely to be at the surface than SO_4^{2-}. Given that $SO_3^{\bullet-}$ needs to react with O_2 for the oxidation to proceed (see Supporting Information, Mechanisms) while sulfate is an inhibitor of S(IV) oxidation, this relative surface propensity of the radical anion creates more favorable reaction conditions at the surface compared to the bulk.[9] Additionally, it has been noted that TMIs themselves can be oxidized or undergo complexation during the S(IV) oxidation process, which would slow down sulfate formation.[19] Since Fe^{3+} and Mn^{2+} are more highly charged than the radicals that propagate the reaction, it is possible that TMIs initiate the process from the core of the aerosol and then an accelerated propagation happens with

https://doi.org/10.1021/acs.est.1c01932
Environ. Sci. Technol. XXXX, XXX, XXX–XXX

radicals and O_2 at the aerosol surface. However, the authors emphasize that the complexity of urban aerosols, including very high ionic strengths (>10 M) and the presence of inhibiting organics (Figure S10) may create conditions favoring a different mechanism in the real world.

Another key aspect of surface access is interaction with spontaneously generated hydrogen peroxide. Lee et al. showed that supermicron pure water droplets generated ca. 30 μM H_2O_2 without application of an external catalyst or voltage, which they attribute to OH radical action at the interface.[46] Since H_2O_2 is a powerful oxidizer of the S(IV) reaction, even these low concentrations could contribute toward reaction acceleration, especially over timescales of minutes if H_2O_2 is continuously generated. Using H_2O_2 production data from Lee et al.,[46] literature S(IV) oxidation rate data at our ionic strength,[47] and assuming that the rate law from dilute solutions holds for concentrated S(IV) samples, an oxidation rate of 0.043 m/min could be obtained (details in the Supporting Information). Furthermore, the production of H_2O_2 at the interface could be enhanced by the presence of radical intermediates involved in S(IV) oxidation, and the hypothesis that the OH radical plays a role in this H_2O_2 generation is consistent with our observation that AAFs are higher at higher pH since it is proposed that OH radicals can be generated from hydroxide ions.[46]

4.3. Aerosol pH. We confirmed the pH of the generated aerosols utilizing substrate deposition onto pH paper as described in previous studies (see Figure S7 in the Supporting Information);[26,48,49] however, the individual environments within these aerosols may be varied. Indeed, it is possible that a pH gradient exists inside aerosols, creating droplets with more basic cores and more acidic surfaces.[50] Although gradients as large as 3.6 pH units have been reported, given how sensitive the reaction is to changes in pH, even a gradient of less than 1 pH unit could explain aerosol-phase acceleration for $S(IV)_{aq}$ oxidation.[10,50] This is partly due to the greatly enhanced reactivity of $Fe(H_2O)_5(OH)^{2+}$ compared to $Fe(H_2O)_6^{3+}$, key complexes for the iron-catalyzed reaction, with the former more present at higher pH.[44] Thus, if a gradient does exist in aerosols, then aerosols are ideal reactors for S(IV) oxidation since the process at interfaces is faster at low pH, while the process in the bulk is potentially faster at high pH (although conflicting kinetic orders for H^+ at pH above 4 have been reported).[9−11,51]

The existence of an aerosol pH gradient is still under debate,[50,52] but it is worth noting that the investigators who proposed it were working with alkaline aerosols, and here we observe larger AAFs for more basic droplets. It is possible that the gradient is an absolute proton concentration difference between the droplet core and surface. In that case, since pH is a logarithmic scale, the pH gradient would be larger at lower proton concentrations. If protons have an inherent surface propensity, then at lower concentrations, a greater fraction of the protons would be able to accumulate at the surface.[41,53] A visual representation for our hypotheses for aerosol-phase acceleration is given in Figure 5.

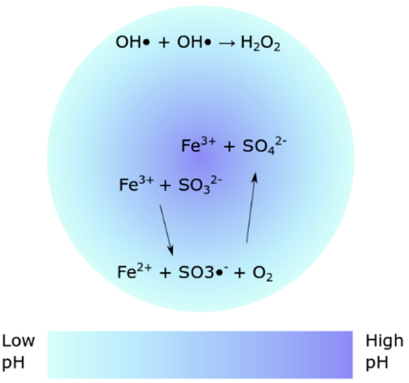

Figure 5. Visual representation of the various factors that contribute to aerosol-phase reaction acceleration. H_2O_2 generation is enhanced at the interface. A pH gradient creates a more acidic surface and more basic core, which favors faster reaction conditions (e.g., the reaction at the bottom of the aerosol is the combination of mechanistic steps given in eqs S7 and S8 and requires a proton to proceed). Highly charged TMIs and inhibiting products are spatially co-located in the aerosol core, while lower charged TMIs, radicals, and O_2 concentrate and react at the interface. Detailed mechanistic steps are omitted from this conceptual image.

4.4. Control of Experimental Variables. There are several precautions that should be taken in reporting droplet-phase reaction acceleration. A recent report by Rovelli et al. provided six recommendations for such studies.[40] Our work was consistent with these recommendations as follows. We controlled solvent evaporation by maintaining the RH in the AOT. Our droplet sizes and reagent concentrations were precisely known by radius and refractive index data derived from the spectral WGMs. We performed experiments on varying concentrations within the range of instrumental detection. The reaction timescale was controlled because the reaction was slow enough that nebulization time was negligible. Online detection of products was obtained by collecting Raman spectra every second. Finally, by working at high pH and not using ionizing nebulizers, we avoided competing gas-phase SO_2 reactions. Therefore, while our experimental design does require the use of relatively high reagent concentrations, we are able to effectively measure acceleration by obtaining kinetics data for individual droplets in well-controlled environments and circumvent several complications that are more common in electrospray experiments. Haan et al. has shown kinetic enhancement in uncharged drying droplets, and most other studies of reaction acceleration use charged droplets.[35,54] Our results are thus unique in that they demonstrate aerosol-phase rate enhancement in single uncharged droplets maintained at constant, high RH where the concentration of reagents over time does not contribute to reaction acceleration.

4.5. Atmospheric Implications. S(IV) oxidation has become a topic of renewed interest due to observations of severe haze events that cannot be explained based on current knowledge from bulk-phase kinetics parameters.[6,7] Laboratory experiments to explain these field observations are now being reported in the literature. For example, Zhang et al. performed smog chamber studies and found that SO_2 oxidation is 2 orders of magnitude faster in aerosol water than in the bulk,[11] which is in agreement with the AAFs we report here. Their studies were performed at lower pH values than we used (0.4−5.0), using much higher TMI concentrations and ppb level SO_2 concentrations. Therefore, their data reflect a combination of both the interface-driven oxidation of SO_2, which is highly efficient at low pH, and the aqueous phase process.[51] Our data thus confirm that droplet-phase acceleration occurs for the aqueous phase process in the absence of SO_2 even at high S(IV) concentrations and at the low TMI concentrations found in the atmosphere.

https://doi.org/10.1021/acs.est.1c01932
Environ. Sci. Technol. XXXX, XXX, XXX−XXX

Furthermore, while most previous studies have been performed at low pH, our data for alkaline and neutral droplets show that accelerated S(IV) oxidation is expected for higher pH aerosols found in some portions of the world.[3,24] By demonstrating that our AAFs exceed what can be obtained from aerosol-phase enrichment alone, we have shown that distinct surface-driven mechanisms may dominate in aerosols, and control of surface area to volume ratios is essential in investigating the kinetics of this process. On a more fundamental level, our results show that inorganic oxidation processes can be accelerated in uncharged aerosols. This complements the many recent findings of organic accelerated reactions measured in electrospray experiments and encourages the use of aerosols in green synthesis and industrial catalysis.

We have shown that TMI-catalyzed S(IV) oxidation is significantly accelerated in the aerosol phase. This is a key step forward in understanding the process of atmospheric S(IV) oxidation, as we have decoupled the interfacial and aqueous reactions and definitively shown the latter to be enhanced in the aerosol phase beyond what can be explained by the salting-in of gases. In addition, we have shown how to quantify chemical reaction acceleration in uncharged droplets of constant size measured on a single aerosol particle basis.

■ ASSOCIATED CONTENT

Supporting Information

The Supporting Information is available free of charge at https://pubs.acs.org/doi/10.1021/acs.est.1c01932.

Additional details of experimental methods; diffusion limitation considerations for the bulk; enrichment of TMIs and S(IV); propagation of error; operative reaction mechanisms; rate calculation; upper limit of hydrogen peroxide contribution; representative behavior of internal standards; higher concentration data showing S(IV) bands in the spectra; nitrate calibration curves; bulk sulfate calibration curve; TMI and S(IV) concentration impacts; aerosol measurements demonstrating the impact of anions; nebulization impact on pH; sample AOT concentration distribution; conductivity calibration curves; representative spectra from ethanol quenching experiments; demonstration of the importance of O2 in the AOT chamber; and conditions used for each experiment (PDF)

■ AUTHOR INFORMATION

Corresponding Author

Vicki H. Grassian − *Department of Chemistry and Biochemistry, University of California San Diego, La Jolla, California 92093, United States;* orcid.org/0000-0001-5052-0045; Email: vhgrassian@ucsd.edu

Authors

Kyle J. Angle − *Department of Chemistry and Biochemistry, University of California San Diego, La Jolla, California 92093, United States*

Erin E. Neal − *Department of Chemistry and Biochemistry, University of California San Diego, La Jolla, California 92093, United States*

Complete contact information is available at: https://pubs.acs.org/10.1021/acs.est.1c01932

Author Contributions

The manuscript was written through the contributions of all authors.

Funding

This material is based upon work supported by the National Science Foundation under Grant AGS1702488. Any opinions, findings, and conclusions or recommendations expressed in this material are those of the authors and do not necessarily reflect the views of the National Science Foundation.

Notes

The authors declare no competing financial interest.

■ ACKNOWLEDGMENTS

The authors thank Neal Arakawa (Environmental and Complex Analysis Laboratory, UCSD) for ICP−MS assistance and John Weeks (Wavemetrics) for providing support and files for Igor Pro fitting analysis.

■ REFERENCES

(1) Fioletov, V. E.; Mclinden, C. A.; Krotkov, N.; Li, C.; Joiner, J.; Theys, N.; Carn, S.; Moran, M. D. A Global Catalogue of Large SO_2 Sources and Emissions Derived from the Ozone Monitoring Instrument. *Atmos. Chem. Phys.* **2016**, *16*, 11497−11519.

(2) Forbes, P. B. C.; Garland, R. M. Outdoor Air Pollution. *Compr. Anal. Chem.* **2016**, *73*, 73−96.

(3) Pye, H. O. T.; Nenes, A.; Alexander, B.; Ault, A. P.; Barth, M. C.; Clegg, S. L.; Collett, J. L.; Fahey, K. M.; Hennigan, C. J.; Herrmann, H.; Kanakidou, M.; Kelly, J. T.; Ku, I.-T.; Mcneill, V. F.; Riemer, N.; Schaefer, T.; Shi, G.; Tilgner, A.; Walker, J. T.; Wang, T.; Weber, R.; Xing, J.; Zaveri, R. A.; Zuend, A. The Acidity of Atmospheric Particles and Clouds. *Atmos. Chem. Phys.* **2020**, *20*, 4809−4888.

(4) Freedman, M. A.; Ott, E.-J. E.; Marak, K. E. Role of pH in Aerosol Processes and Measurement Challenges. *J. Phys. Chem. A* **2019**, *123*, 1275−1284.

(5) Duan, J.; Lyu, R.; Wang, Y.; Xie, X.; Wu, Y.; Tao, J.; Cheng, T.; Liu, Y.; Peng, Y.; Zhang, R.; He, Q.; Ga, W.; Zhang, X.; Zhang, Q. Particle Liquid Water Content and Aerosol Acidity Acting as Indicators of Aerosol Activation Changes in Cloud Condensation Nuclei (CCN) during Pollution Eruption in Guangzhou of South China. *Aerosol Air Qual. Res.* **2019**, *9*, 2662−2670.

(6) Wang, Y.; Zhang, Q.; Jiang, J.; Zhou, W.; Wang, B.; He, K.; Duan, F.; Zhang, Q.; Philip, S.; Xie, Y. Enhanced Sulfate Formation during China's Severe Winter Haze Episode in January 2013 Missing from Current Models. *J. Geophys. Res.: Atmos.* **2014**, *119*, 425.

(7) Zheng, B.; Zhang, Q.; Zhang, Y.; He, K. B.; Wang, K.; Zheng, G. J.; Duan, F. K.; Ma, Y. L.; Kimoto, T. Heterogeneous Chemistry: A Mechanism Missing in Current Models to Explain Secondary Inorganic Aerosol Formation during the January 2013 Haze Episode in North China. *Atmos. Chem. Phys.* **2015**, *15*, 2031−2049.

(8) Connick, R. E.; Zhang, Y.-X.; Lee, S.; Adamic, R.; Chieng, P. Kinetics and Mechanism of the Oxidation of HSO_3^- by O_2. 1. the Uncatalyzed Reaction. *Inorg. Chem.* **1995**, *34*, 4543−4553.

(9) Martin, L. R.; Hill, M. W.; Tai, A. F.; Good, T. W. The Iron Catalyzed Oxidation of Sulfur(IV) in Aqueous Solution: Differing Effects of Organics at High and Low PH. *J. Geophys. Res.* **1991**, *96*, 3085.

(10) Brandt, C.; van Eldik, R. Transition Metal-Catalyzed Oxidation of Sulfur(IV) Oxides: Atmospheric-Relevant Processes and Mechanisms. *Chem. Rev.* **1995**, *95*, 119−190.

(11) Zhang, H.; Xu, Y.; Jia, L. A Chamber Study of Catalytic Oxidation of SO_2 by Mn^{2+}/Fe^{3+} in Aerosol Water. *Atmos. Environ.* **2021**, *245*, 118019.

(12) Turšič, J.; Grgić, I.; Podkrajšek, B. Influence of Ionic Strength on Aqueous Oxidation of SO_2 Catalyzed by Manganese. *Atmos. Environ.* **2003**, *37*, 2589−2595.

(13) Connick, R. E.; Zhang, Y.-X. Kinetics and Mechanism of the Oxidation of HSO_3^- by O_2. 2. the Manganese(II)-Catalyzed Reaction. *Inorg. Chem.* **1996**, *35*, 4613−4621.
(14) Tao, W.; Su, H.; Zheng, G.; Wang, J.; Wei, C.; Liu, L.; Ma, N.; Li, M.; Zhang, Q.; Pöschl, U.; Cheng, Y. Aerosol pH and Chemical Regimes of Sulfate Formation in Aerosol Water during Winter Haze in the North China Plain. *Atmos. Chem. Phys.* **2020**, *20*, 11729−11746.
(15) Clarke, A. G.; Radojevic, M. Oxidation of SO_2 in Rainwater and Its Role in Acid Rain Chemistry. *Atmos. Environ.* **1987**, *21*, 1115−1123.
(16) Bertram, T. H.; Cochran, R. E.; Grassian, V. H.; Stone, E. A. Sea Spray Aerosol Chemical Composition: Elemental and Molecular Mimics for Laboratory Studies of Heterogeneous and Multiphase Reactions. *Chem. Soc. Rev.* **2018**, *47*, 2374−2400.
(17) Liu, T.; Chan, A. W. H.; Abbatt, J. P. D. Multiphase Oxidation of Sulfur Dioxide in Aerosol Particles: Implications for Sulfate Formation in Polluted Environments. *Environ. Sci. Technol.* **2021**, *55*, 4242.
(18) Yermakov, A. N.; Purmal, A. P. Iron-Catalyzed Oxidation of Sulfite: From Established Results to a New Understanding. *Prog. React. Kinet. Mech.* **2003**, *28*, 189−256.
(19) Warneck, P. The Oxidation of Sulfur(IV) by Reaction with Iron(III): A Critical Review and Data Analysis. *Phys. Chem. Chem. Phys.* **2018**, *20*, 4020−4037.
(20) The Merck Index Online - chemicals, drugs and biologicals. https://www.rsc.org/merck-index (accessed Apr 22, 2020).
(21) Preston, T. C.; Reid, J. P. Accurate and Efficient Determination of the Radius, Refractive Index, and Dispersion of Weakly Absorbing Spherical Particle Using Whispering Gallery Modes. *J. Opt. Soc. Am. B* **2013**, *30*, 2113.
(22) Rafferty, A.; Gorkowski, K.; Zuend, A.; Preston, T. C. Optical Deformation of Single Aerosol Particles. *Proc. Natl. Acad. Sci. U.S.A.* **2019**, *116*, 19880−19886.
(23) Coddens, E. M.; Angle, K. J.; Grassian, V. H. Titration of Aerosol pH through Droplet Coalescence. *J. Phys. Chem. Lett.* **2019**, *10*, 4476−4483.
(24) Mudgal, P. K.; Sharma, A. K.; Mishra, C. D.; Bansal, S. P.; Gupta, K. S. Kinetics of Ammonia and Ammonium Ion Inhibition of the Atmospheric Oxidation of Aqueous Sulfur Dioxide by Oxygen. *J. Atmos. Chem.* **2008**, *61*, 31−55.
(25) Manoj, S. V.; Gupta, K. S.; Mudgal, P. K. Kinetics of Iron(III)-Catalyzed Autoxidation of Sulfur(IV) in Acetate Buffered Medium. *Transition Met. Chem.* **2008**, *33*, 311−316.
(26) Angle, K. J.; Crocker, D. R.; Simpson, R. M. C.; Mayer, K. J.; Garofalo, L. A.; Moore, A. N.; Mora Garcia, S. L.; Or, V. W.; Srinivasan, S.; Farhan, M.; Sauer, J. S.; Lee, C.; Pothier, M. A.; Farmer, D. K.; Martz, T. R.; Bertram, T. H.; Cappa, C. D.; Prather, K. A.; Grassian, V. H. Acidity across the Interface from the Ocean Surface to Sea Spray Aerosol. *Proc. Natl. Acad. Sci. U.S.A.* **2021**, *118*, No. e2018397118.
(27) Beyad, Y.; Burns, R.; Puxty, G.; Maeder, M. A Speciation Study of Sulfur(IV) in Aqueous Solution. *Dalton Trans.* **2014**, *43*, 2147−2152.
(28) Millero, F. J.; Yao, W.; Aicher, J. The Speciation of Fe(II) and Fe(III) in Natural Waters. *Mar. Chem.* **1995**, *50*, 21−39.
(29) Hem, J. D. Chemical Equilibria Affecting the Behavior of Manganese in Natural Water. *Bull. Int. Assoc. Sci. Hydrol.* **1963**, *8*, 30−37.
(30) Liu, T.; Clegg, S. L.; Abbatt, J. P. D. Fast Oxidation of Sulfur Dioxide by Hydrogen Peroxide in Deliquesced Aerosol Particles. *Proc. Natl. Acad. Sci. U.S.A.* **2020**, *117*, 1354−1359.
(31) Boyer, H. C.; Gorkowski, K.; Sullivan, R. C. In Situ pH Measurements of Individual Levitated Microdroplets Using Aerosol Optical Tweezers. *Anal. Chem.* **2020**, *92*, 1089−1096.
(32) Tang, I. N.; Tridico, A. C.; Fung, K. H. Thermodynamic and Optical Properties of Sea Salt Aerosols. *J. Geophys. Res.: Atmos.* **1997**, *102*, 23269−23275.
(33) Tang, I. N.; Munkelwitz, H. R. Water Activities, Densities, and Refractive Indices of Aqueous Sulfates and Sodium Nitrate Droplets of Atmospheric Importance. *J. Geophys. Res.* **1994**, *99*, 18801−18808.
(34) Bao, Z.-C.; Barker, J. R. Temperature and Ionic Strength Effects on Some Reactions Involving Sulfate Radical $[SO_4^-(Aq)]$. *J. Phys. Chem.* **1996**, *100*, 9780−9787.
(35) Wei, Z.; Li, Y.; Cooks, R. G.; Yan, X. Accelerated Reaction Kinetics in Microdroplets: Overview and Recent Developments. *Annu. Rev. Phys. Chem.* **2020**, *71*, 31−51.
(36) Lee, J. K.; Samanta, D.; Nam, H. G.; Zare, R. N. Micrometer-Sized Water Droplets Induce Spontaneous Reduction. *J. Am. Chem. Soc.* **2019**, *141*, 10585−10589.
(37) Banerjee, S.; Gnanamani, E.; Yan, X.; Zare, R. N. Can All Bulk-Phase Reactions Be Accelerated in Microdroplets? *Analyst* **2017**, *142*, 1399−1402.
(38) Clarke, A. G.; Radojevic, M. Oxidation Rates of SO_2 in Sea-Water and Sea-Salt Aerosols. *Atmos. Environ.* **1984**, *18*, 2761−2767.
(39) Wang, W.; Liu, M.; Wang, T.; Song, Y.; Zhou, L.; Cao, J.; Hu, J.; Tang, G.; Chen, Z.; Li, Z.; Xu, Z.; Peng, C.; Lian, C.; Chen, Y.; Pan, Y.; Zhang, Y.; Sun, Y.; Li, W.; Zhu, T.; Tian, H.; Ge, M. Sulfate Formation Is Dominated by Manganese-Catalyzed Oxidation of SO_2 on Aerosol Surfaces during Haze Events. *Nat. Commun.* **2021**, *12*, 1993.
(40) Rovelli, G.; Jacobs, M. I.; Willis, M. D.; Rapf, R. J.; Prophet, A. M.; Wilson, K. R. A Critical Analysis of Electrospray Techniques for the Determination of Accelerated Rates and Mechanisms of Chemical Reactions in Droplets. *Chem. Sci.* **2020**, *11*, 13026.
(41) Wilson, K. R.; Prophet, A. M.; Rovelli, G.; Willis, M. D.; Rapf, R. J.; Jacobs, M. I. A Kinetic Description of How Interfaces Accelerate Reactions in Micro-Compartments. *Chem. Sci.* **2020**, *11*, 8533−8545.
(42) Eriksen, T. Self-Diffusion Studies in Aqueous Sulfite Solutions. *Chem. Eng. Sci.* **1967**, *22*, 727−736.
(43) Das, T. N. Reactivity and Role of $SO_5^{\bullet-}$ Radical in Aqueous Medium Chain Oxidation of Sulfite to Sulfate and Atmospheric Sulfuric Acid Generation. *J. Phys. Chem. A* **2001**, *105*, 9142−9155.
(44) Luo, M.; Wauer, N. A.; Angle, K. J.; Dommer, A. C.; Song, M.; Nowak, C. M.; Amaro, R. E.; Grassian, V. H. Insights into the Behavior of Nonanoic Acid and Its Conjugate Base at the Air/Water Interface through a Combined Experimental and Theoretical Approach. *Chem. Sci.* **2020**, *11*, 10647−10656.
(45) Ruiz-Lopez, M. F.; Francisco, J. S.; Martins-Costa, M. T. C.; Anglada, J. M. Molecular Reactions at Aqueous Interfaces. *Nat. Rev. Chem.* **2020**, *4*, 459−475.
(46) Lee, J. K.; Walker, K. L.; Han, H. S.; Kang, J.; Prinz, F. B.; Waymouth, R. M.; Nam, H. G.; Zare, R. N. Spontaneous Generation of Hydrogen Peroxide from Aqueous Microdroplets. *Proc. Natl. Acad. Sci. U.S.A.* **2019**, *116*, 19294−19298.
(47) Maaß, F.; Elias, H.; Wannowius, K. J. Kinetics of the Oxidation of Hydrogen Sulfite by Hydrogen Peroxide in Aqueous Solution: Ionic Strength Effects and Temperature Dependence. *Atmos. Environ.* **1999**, *33*, 4413−4419.
(48) Craig, R. L.; Peterson, P. K.; Nandy, L.; Lei, Z.; Hossain, M. A.; Camarena, S.; Dodson, R. A.; Cook, R. D.; Dutcher, C. S.; Ault, A. P. Direct Determination of Aerosol pH: Size-Resolved Measurements of Submicrometer and Supermicrometer Aqueous Particles. *Anal. Chem.* **2018**, *90*, 11232−11239.
(49) Li, G.; Su, H.; Ma, N.; Zheng, G.; Kuhn, U.; Li, M.; Klimach, T.; Pöschl, U.; Cheng, Y. Multifactor Colorimetric Analysis on pH-Indicator Papers: An Optimized Approach for Direct Determination of Ambient Aerosol pH. *Atmos. Meas. Tech.* **2020**, *13*, 6053−6065.
(50) Wei, H.; Vejerano, E. P.; Leng, W.; Huang, Q.; Willner, M. R.; Marr, L. C.; Vikesland, P. J. Aerosol Microdroplets Exhibit a Stable pH Gradient. *Proc. Natl. Acad. Sci. U.S.A.* **2018**, *115*, 7272−7277.
(51) Hung, H.-M.; Hsu, M.-N.; Hoffmann, M. R. Quantification of SO_2 Oxidation on Interfacial Surfaces of Acidic Micro-Droplets: Implication for Ambient Sulfate Formation. *Environ. Sci. Technol.* **2018**, *52*, 9079−9086.

https://doi.org/10.1021/acs.est.1c01932
Environ. Sci. Technol. XXXX, XXX, XXX−XXX

(52) Colussi, A. J. Can the pH at the Air/Water Interface Be Different from the pH of Bulk Water? *Proc. Natl. Acad. Sci. U.S.A.* **2018**, *115*, No. E7887.
(53) Das, S.; Imoto, S.; Sun, S.; Nagata, Y.; Backus, E. H. G.; Bonn, M. Nature of Excess Hydrated Proton at the Water-Air Interface. *J. Am. Chem. Soc.* **2020**, *142*, 945−952.
(54) Haan, D. O. D.; Corrigan, A. L.; Smith, K. W.; Stroik, D. R.; Turley, J. J.; Lee, F. E.; Tolbert, M. A.; Jimenez, J. L.; Cordova, K. E.; Ferrell, G. R. Secondary Organic Aerosol-Forming Reactions of Glyoxal with Amino Acids. *Environ. Sci. Technol.* **2009**, *43*, 2818−2824.

https://doi.org/10.1021/acs.est.1c01932
Environ. Sci. Technol. XXXX, XXX, XXX−XXX